A Simple and Robust Method to Quantify Exciton Dissociation Efficiency with High Precision in Non-Fullerene Organic Solar Cells

Jared Faisst,[1,2,3,*] Mathias List,[1,3] Leonie Pap,[1,3] Reid Patterson,[1,3] Uli Würfel,[1,3] and Andreas W. Bett[1,2,†]

[1] *Fraunhofer Institute for Solar Energy Systems ISE, Heidenhofstr. 2, 79110 Freiburg, Germany*

[2] *Institute of Physics, University of Freiburg, Hermann-Herder-Str. 3, 79104 Freiburg, Germany*

[3] *Freiburg Materials Research Center FMF, University of Freiburg, Stefan-Meier-Str. 21, 79104 Freiburg, Germany*

[*] jared.faisst@ise.fraunhofer.de

[†] andreas.bett@ise.fraunhofer.de

S1. CHEMICAL DEFINITIONS

- **D18:Y6**
  - **D18**: Poly[dithieno[3',2':3,4;2",3":5,6]benzo[1,2-c][1,2,5]thiadiazole(DTBT)]; purchased from *1-Material*

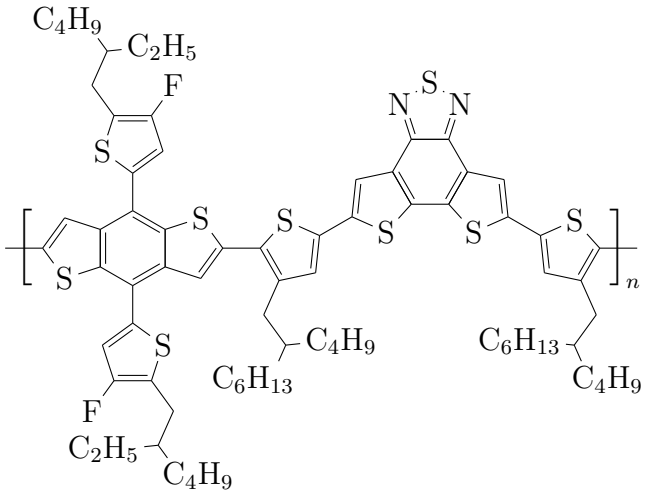

  - **Y6**

    2,2'-[[12,13-Bis(2-butyloctyl)-12,13-dihydro-3,9-2,2'-[[12,13-Bis(2-ethylhexyl)-12,13-dihydro-3,9-diundecylbisthieno[2",3":4',5']thieno[2',3':4,5]pyrrolo[3,2-e:2',3'-g][2,1,3]benzothiadiazole-2,10-diyl]bis[methylidyne(5,6-difluoro-3-oxo-1H-indene-2,1(3H)-diylidene)]]bis[propanedinitrile]; purchased from *1-Material*

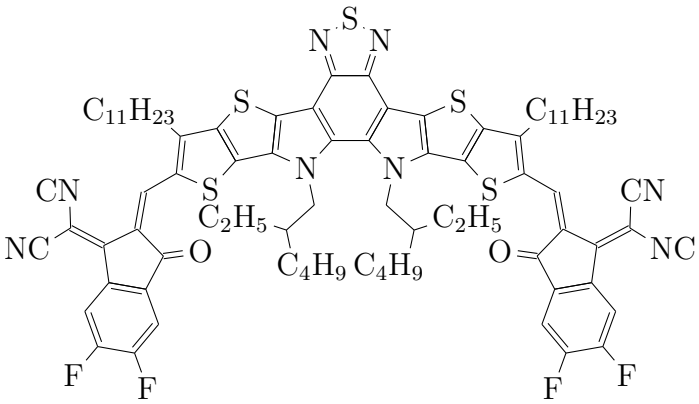

- PM6:DTY6
  - PBDB-T-2F (**PM6**): Poly[(2,6-(4,8-bis(5-(2-ethylhexyl-3-fluoro)thiophen-2-yl)-benzo[1,2-b:4,5-b']dithiophene))-alt-(5,5-(1',3'-di-2-thienyl-5',7'-bis(2-ethylhexyl)benzo[1',2'-c:4',5'-c']dithiophene-4,8-dione)]; purchased from *1-Material*

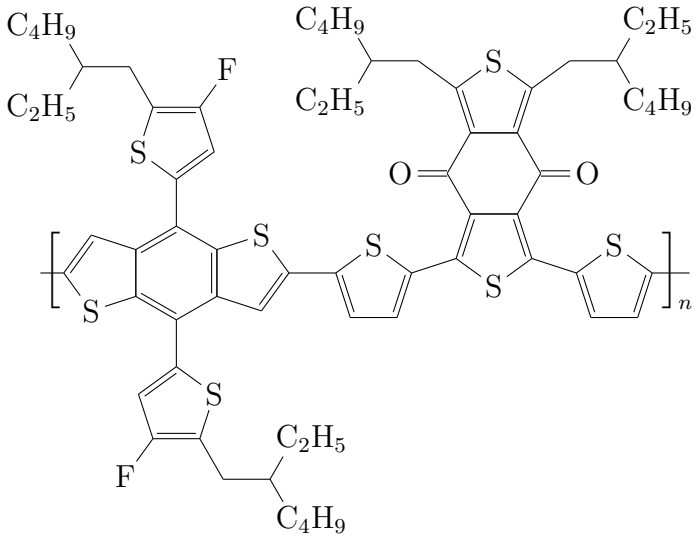

– BTP-4F-24 (**DTY6**): 2,2'-((2Z,2'Z)-((12,13-bis(2-decylteradecyl)-3,9-diundecyl-12,13-dihydro-[1,2,5]thiadiazolo[3,4-e]thieno[2",3":4',5']thieno[2',3':4,5]pyrrolo[3,2-g]thieno[2',3':4,5]thieno[3,2-b]indole-2,10-diyl)bis(methanylylidene))bis(5,6-difluoro-3-oxo-2,3-dihydro-1H-indene-2,1-diylidene))dimalononitrile; purchased from *1-Material*

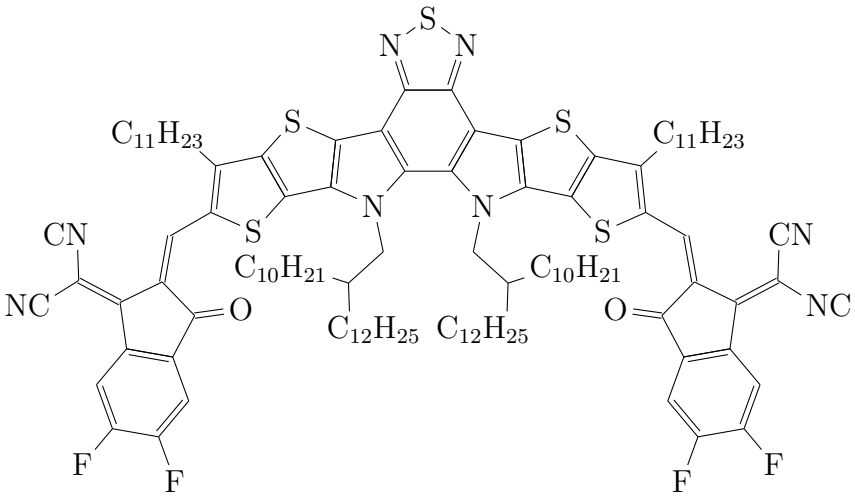

S2. SOLAR CELL FABRICATION

The solar cells were built according to the stack ITO/PEDOT:PSS/PAL/PDIN/Silver using glass substrates (25 mm × 25 mm × 1 mm). The substrates were cleaned in ultrasonic baths of acetone, isopropanol and deionized water. For the transparent bottom electrode, Indium Tin Oxide (ITO) was deposited via sputtering to achieve a thickness of 170 nm. PALs were processed via spin coating under nitrogen atmosphere. D18:Y6 was dissolved with a

concentration of $9\,\mathrm{mg\,mL^{-1}}$ in chloroform and PM6:DTY6 with $16\,\mathrm{mg\,mL^{-1}}$ in o-xylene, both with the varying donor:acceptor ratios as provided in the main manuscript.

The blends were deposited via spin-coating. Serving as an electron transport layer, PDIN (purchased from Ossila) was dissolved in methanol with a concentration of $2\,\mathrm{mg\,mL^{-1}}$, adding 0.3 vol% acetic acid (p.a. grade from Sigma Aldrich). It was deposited via spin-coating at 4000 rpm producing a 6 nm thick layer. Finally, a 100 nm thick layer of silver was deposited via thermal evaporation at a pressure of $< 5 \times 10^{-5}\,\mathrm{mbar}$. The active area of a solar cell reads $0.0925\,\mathrm{cm^2}$, limited by the contact area of the electrodes silver and ITO, respectively.

S3. CURRENT-VOLTAGE CHARACTERISTICS

The current-voltage curves were recorded with a Keithley 2400 sourcemeter while illuminated with a sun simulator (Newport SP94063A-SR1-167, simulated AM1.5G, corrected for spectral mismatch). The cells were measured under nitrogen atmosphere at room temperature (kept approximately constant via fan). The JV sweeps were performed from $-1\,\mathrm{V}$ to $1\,\mathrm{V}$ obtaining 50 data points with dwell times of 50 ms and integrating over 1 NPLC (20 ms).

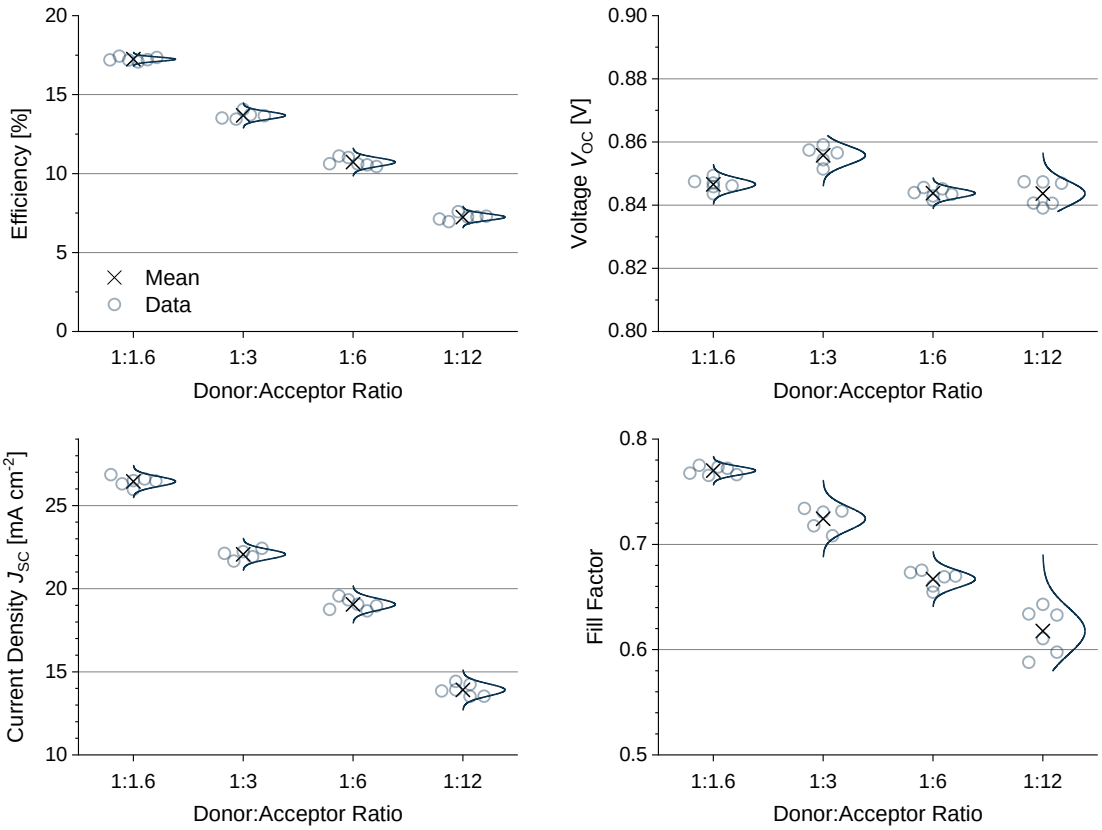

FIG. S1: Figures of merit for the D18:Y6 solar cells.

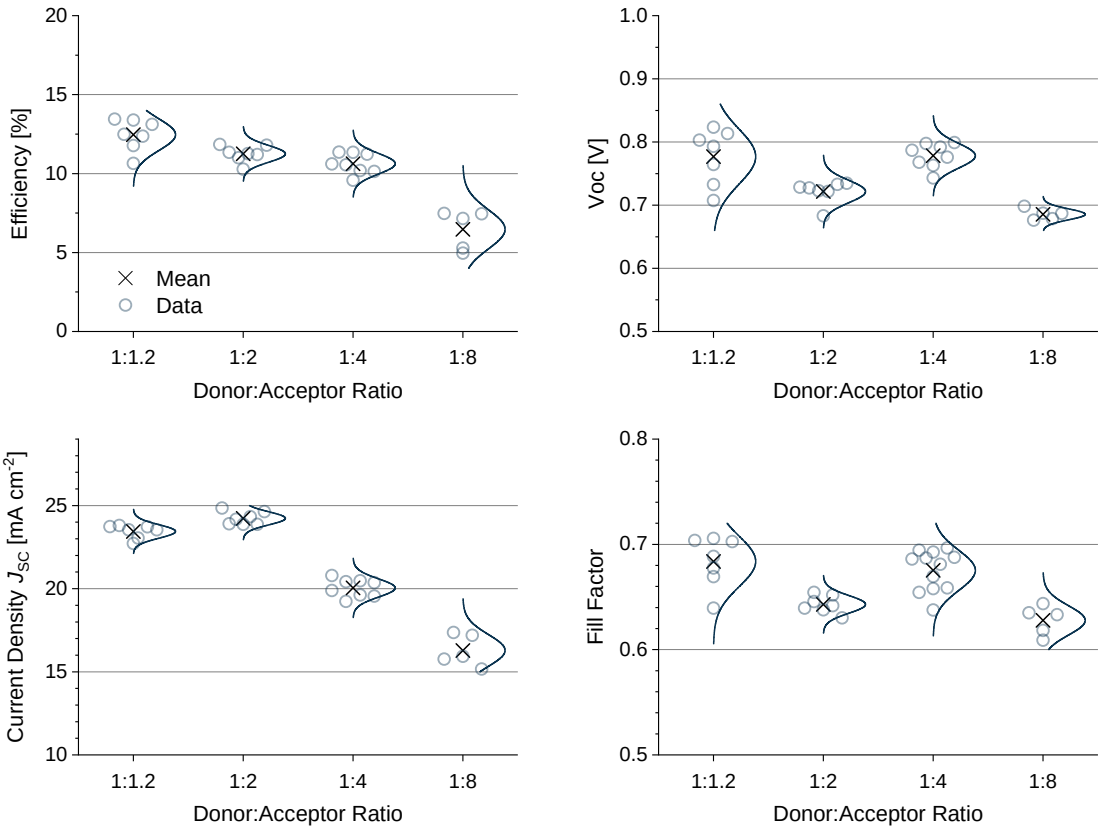

FIG. S2: Figures of merit for the PM6:DTY6 solar cells.

S4. PHOTOLUMINESCENCE MEASUREMENTS

All photoluminescence (PL) measurements were performed under inert atmosphere. For steady-state PL characterization, the devices were illuminated with a continuous-wave 532 nm laser. The beam was expanded using a TopHat beam converter to ensure homogeneous illumination of the active area. The emitted PL was filtered using a 600 nm long-pass filter and directed onto the entrance slit of a Czerny–Turner spectrograph (*Andor Shamrock 193i*) equipped with an InGaAs photodiode array detector (*Andor iDus DU490A*) cooled to −50 °C. Spectral response correction was applied using a calibrated tungsten reference lamp measured by *Fraunhofer CalLab PV Cells*. The excitation intensity corresponding to "1 sun" equivalent illumination was determined by adjusting the laser power such that the measured short-circuit current density (J_{SC}) matched that obtained under solar simulator illumination (AM1.5G, corrected for spectral mismatch).

S5. OPTICAL MEASUREMENTS AND SIMULATIONS

Optical properties and current generation were simulated using the transfer matrix method as implemented in the *CODE/SCOUT* software package developed by W. Theiss. This method simulates light propagation through multiple layers, accounting for multiple reflections at interfaces and interference effects. This approach enables accurate modeling of reflectance (R), transmittance (T), and absorptance (A) spectra.

Experimentally, reflection, transmission, and absorption spectra were recorded in the wavelength range of 280–1200 nm using a *PerkinElmer Lambda 950 UV/Vis/NIR* spectrophotometer equipped with an integrating sphere. Single layers of each material were prepared on glass substrates, and their thicknesses were determined using a *Veeco Dektak 150* stylus profilometer.

Based on these measurements, the complex refractive index spectra (n and k) were parameterized by fitting a Kim oscillator model in *SCOUT*. The obtained complex refractive indices were then imported into a multilayer model representing the full solar cell stack. From this model, the wavelength-dependent absorptance of the photoactive layer, $A_{\mathrm{PAL}}(\lambda)$, was obtained.

S6. RESULTS FOR EXCITON DISSOCIATION EFFICIENCY WITH THE DONOR-ACCEPTOR VARIATION USING SIMULATED LAYER ABSORPTANCE

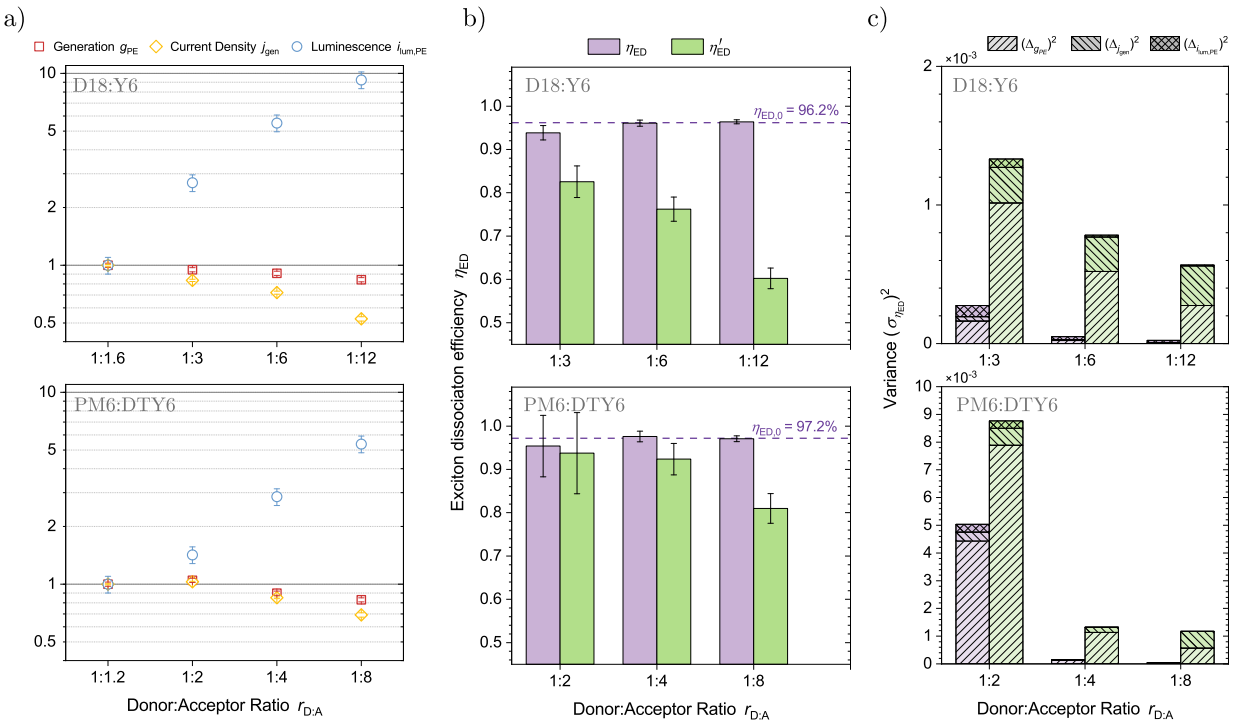

FIG. S3: Similar to Figure 5 in the main manuscript: Results for D18:Y6 (top row) and PM6:DTY6 (bottom row). (a) Evolution of the normalized quantities: integrated photogeneration of excitons g_{PE} (red) from layer absorptance simulation, generated current density j_{gen} (yellow), and exciton photoluminescence $i_{lum,PE}$ (blue) as a function of the donor–acceptor ratio. (b) Exciton dissociation efficiencies of the reference devices (η_{ED}, purple) and the comparative devices (η'_{ED}, green), with the weighted mean shown as a dashed line. (c) Variance analysis of the values shown in (b), with the contributing uncertainty components from g_{PE}, j_{gen}, and $i_{lum,PE}$ encoded in the stacked bars. The results for the weighted mean of the obtained η_{ED} values are 96.2 ± 0.4 for D18:Y6 and 97.2 ± 0.6 for PM6:DTY6.

S7. ERROR ESTIMATION FOR EXCITON DISSOCIATION EFFICIENCIES

The uncertainty in the calculated exciton dissociation efficiencies η_{ED} and η'_{ED} was evaluated by Gaussian error propagation. For all quantities, the standard deviations σ_x were determined from either repeated experimental measurements ($i_{lum,PE}$ and j_{gen}) or from systematic deviation if exceeding the statistical uncertainty (g_{PE}, see main text). According to the Gaussian law of error propagation, the total variance of η_{ED} is obtained as the quadratic

sum of all independent contributions:

$$\sigma^2_{\eta_{\mathrm{ED}}} = \underbrace{\left(\frac{\partial \eta_{\mathrm{ED}}}{\partial g_{\mathrm{PE}}}\sigma_{g_{\mathrm{PE}}}\right)^2}_{\Delta^2_{g_{\mathrm{PE}}}} + \underbrace{\left(\frac{\partial \eta_{\mathrm{ED}}}{\partial j_{\mathrm{gen}}}\sigma_{j_{\mathrm{gen}}}\right)^2}_{\Delta^2_{j_{\mathrm{gen}}}} + \underbrace{\left(\frac{\partial \eta_{\mathrm{ED}}}{\partial i_{\mathrm{lum,PE}}}\sigma_{i_{\mathrm{lum,PE}}}\right)^2}_{\Delta^2_{i_{\mathrm{lum,PE}}}}. \tag{1}$$

Here, $\Delta_x = \frac{\partial \eta_{\mathrm{ED}}}{\partial x}\,\sigma_x$ denotes the standard uncertainty contribution from each variable x, and Δ^2_x its corresponding variance contribution, as depicted in Figure 5c of the main manuscript. The total propagated uncertainty is therefore

$$\sigma_{\eta_{\mathrm{ED}}} = \sqrt{\Delta^2_{g_{\mathrm{PE}}} + \Delta^2_{j_{\mathrm{gen}}} + \Delta^2_{i_{\mathrm{lum,PE}}}}\,. \tag{2}$$

Error estimation for the reference efficiency η_{ED}

For the reference morphology, the exciton dissociation efficiency is defined as:

$$\eta_{\mathrm{ED}} = \frac{g_{\mathrm{PE}} - i_{\mathrm{lum,PE}}}{j_{\mathrm{gen}} - i_{\mathrm{lum,PE}}}. \tag{3}$$

The individual variance contributions are then given by:

$$\Delta^2_{g_{\mathrm{PE}}} = \left[\frac{1}{j_{\mathrm{gen}} - i_{\mathrm{lum,PE}}}\sigma_{g_{\mathrm{PE}}}\right]^2, \tag{4}$$

$$\Delta^2_{j_{\mathrm{gen}}} = \left[\frac{i_{\mathrm{lum,PE}} - g_{\mathrm{PE}}}{(j_{\mathrm{gen}} - i_{\mathrm{lum,PE}})^2}\sigma_{j_{\mathrm{gen}}}\right]^2, \tag{5}$$

$$\Delta^2_{i_{\mathrm{lum,PE}}} = \left[\frac{g_{\mathrm{PE}} - j_{\mathrm{gen}}}{(j_{\mathrm{gen}} - i_{\mathrm{lum,PE}})^2}\sigma_{i_{\mathrm{lum,PE}}}\right]^2. \tag{6}$$

Error estimation for the comparative efficiency η'_{ED}

For the comparative morphology, the exciton dissociation efficiency is given by:

$$\eta'_{\mathrm{ED}} = \frac{j_{\mathrm{gen}}}{g_{\mathrm{PE}}} \cdot \frac{g_{\mathrm{PE}} - i_{\mathrm{lum,PE}}}{j_{\mathrm{gen}} - i_{\mathrm{lum,PE}}}. \tag{7}$$

The corresponding variance contributions read:

$$\Delta^2_{g_{\mathrm{PE}}} = \left[\frac{-i_{\mathrm{lum,PE}} j_{\mathrm{gen}}}{g^2_{\mathrm{PE}}(i_{\mathrm{lum,PE}} - j_{\mathrm{gen}})}\sigma_{g_{\mathrm{PE}}}\right]^2, \tag{8}$$

$$\Delta^2_{j_{\mathrm{gen}}} = \left[\frac{i_{\mathrm{lum,PE}}(i_{\mathrm{lum,PE}} - g_{\mathrm{PE}})}{g_{\mathrm{PE}}(j_{\mathrm{gen}} - i_{\mathrm{lum,PE}})^2}\sigma_{j_{\mathrm{gen}}}\right]^2, \tag{9}$$

$$\Delta^2_{i_{\mathrm{lum,PE}}} = \left[\frac{j_{\mathrm{gen}}(g_{\mathrm{PE}} - j_{\mathrm{gen}})}{g_{\mathrm{PE}}(j_{\mathrm{gen}} - i_{\mathrm{lum,PE}})^2}\sigma_{i_{\mathrm{lum,PE}}}\right]^2. \tag{10}$$

S8. WEIGHTED MEAN OF EXCITON DISSOCIATION EFFICIENCY

The weighted mean of the exciton dissociation efficiency, η_{ED}, was determined using inverse-variance weighting, where the individual uncertainties are represented by their standard deviations $\sigma_{\eta_{\mathrm{ED},i}}$:

$$\bar{\eta}_{\mathrm{ED}} = \frac{\sum_i \frac{\eta_{\mathrm{ED},i}}{\sigma^2_{\eta_{\mathrm{ED},i}}}}{\sum_i \frac{1}{\sigma^2_{\eta_{\mathrm{ED},0,i}}}}. \tag{11}$$

The corresponding standard uncertainty of the weighted mean is then given by:

$$\sigma_{\bar{\eta}_{\mathrm{ED}}} = \sqrt{\frac{1}{\sum_i \frac{1}{\sigma^2_{\eta_{\mathrm{ED},0,i}}}}}. \tag{12}$$

Here, each individual measurement $\eta_{\mathrm{ED},0,i}$ is weighted according to the inverse of its variance $\sigma^2_{\eta_{\mathrm{ED},0,i}}$, ensuring that more precise measurements contribute more strongly to the mean.

S9. ERROR PROPAGATION IN CONVENTIONAL OPTICAL SIMULATIONS

The optical simulation approach to directly obtain the reference exciton dissociation efficiency η_{ED} follows:

$$\eta_{\mathrm{ED}} = \frac{J_{\mathrm{gen}}}{J_{\mathrm{gen,PE}}}, \tag{13}$$

where J_{gen} denotes the experimentally derived generation current density (approximated using J_{SC}) and $J_{\mathrm{gen,PE}}$ the simulated generation current density of photogenerated excitons obtained from optical modeling of the layer stack.

To evaluate the uncertainty in η_{ED}, both uncertainties in J_{gen} and $J_{\mathrm{gen,PE}}$ must be considered. The experimental uncertainty $\sigma_{J_{\mathrm{gen}}}$ is symmetric (determined as the standard error on the mean), whereas the simulated current $J_{\mathrm{gen,PE}}$ exhibits an asymmetric uncertainty caused by variations in layer thickness, resulting in unequal deviations for increased or decreased thickness. Accordingly, both quantities are expressed as

$$J_{\mathrm{gen}} = J^0_{\mathrm{gen}} \pm \sigma_{J_{\mathrm{gen}}}, \tag{14}$$

$$J_{\mathrm{gen,PE}} = J^0_{\mathrm{gen,PE}}{}^{+\sigma_{J_{\mathrm{gen,PE},+}}}_{-\sigma_{J_{\mathrm{gen,PE},-}}}. \tag{15}$$

The standard Gaussian error propagation for a quotient yields

$$\frac{\sigma_{\eta_{\mathrm{ED}}}}{\eta_{\mathrm{ED}}} = \sqrt{\left(\frac{\sigma_{J_{\mathrm{gen}}}}{J_{\mathrm{gen}}}\right)^2 + \left(\frac{\sigma_{J_{\mathrm{gen,PE}}}}{J_{\mathrm{gen,PE}}}\right)^2}. \tag{16}$$

To account for the asymmetric uncertainty in the simulated quantity, the upper and lower bounds of $\sigma_{\eta_{\mathrm{ED}}}$ are determined separately, by using the smaller simulated current ($-\sigma_{J_{\mathrm{gen,PE},-}}$) for the upper uncertainty and the larger simulated current ($+\sigma_{J_{\mathrm{gen,PE},+}}$) for the lower uncertainty:

$$\sigma_{\eta_{\mathrm{ED},+}} = \eta_{\mathrm{ED}} \sqrt{\left(\frac{\sigma_{J_{\mathrm{gen}}}}{J_{\mathrm{gen}}}\right)^2 + \left(\frac{\sigma_{J_{\mathrm{gen,PE},-}}}{J_{\mathrm{gen,PE}}}\right)^2}, \tag{17}$$

$$\sigma_{\eta_{\mathrm{ED},-}} = \eta_{\mathrm{ED}} \sqrt{\left(\frac{\sigma_{J_{\mathrm{gen}}}}{J_{\mathrm{gen}}}\right)^2 + \left(\frac{\sigma_{J_{\mathrm{gen,PE},+}}}{J_{\mathrm{gen,PE}}}\right)^2}. \tag{18}$$

Here, $\sigma_{\eta_{\mathrm{ED},+}}$ and $\sigma_{\eta_{\mathrm{ED},-}}$ represent the upper and lower standard uncertainty bounds, respectively.